Received: 18 December 2019 | Revised: 9 March 2020 | Accepted: 20 April 2020

DOI: 10.1002/eqe.3284

RESEARCH ARTICLE

WILEY

Seismic control of rocking structures via external resonators

Xiao Pan[1] | **Christian Málaga-Chuquitaype**[2]

[1]Department of Civil Engineering, University of British Columbia, Vancouver, British Columbia, Canada

[2]Department of Civil and Environmental Engineering, Imperial College London, London, UK

Correspondence
Christian Málaga-Chuquitaype, Department of Civil and Environmental Engineering, Imperial College London, Skempton Building, London SW7 2AZ, UK.
Email: c.malaga@imperial.ac.uk

Summary

Tall rigid blocks are prevalent in ancient historical constructions. Such structures are prone to rocking behaviour under strong ground motion, which is recognizably challenging to predict and mitigate. Our study is motivated by the need to provide innovative nonintrusive solutions to attenuate the rocking response of historical buildings and monuments. In this paper, we examine a novel scheme that employs external resonators buried next to the rocking structure as a means to control its seismic response. The strategy capitalizes on the vibration absorbing potential of the structure-soil-resonator interaction. Furthermore, the benefits of combining the resonators with inerters in order to reduce their gravitational mass without hampering their motion-control capabilities are also explored. Advanced numerical analyses of discrete models under coherent acceleration pulses with rocking bodies of different slenderness ratios under various ground motion intensities highlight the significant vibration absorbing qualities of the external resonating system. The influence of key system parameters such as the mass, stiffness, and damping of the resonator and those of the soil-structure-resonator arrangement are studied. Finally, a case study on the evaluation of the response of rocking structures with external resonators under real pulse-like ground-motion records confirms the important reductions in peak seismic rotational demands obtained with the proposed arrangement.

KEYWORDS

inerter, pulse-like ground motion, resonator, rocking motion, seismic control

1 | INTRODUCTION

The vast cultural significance and value of historical constructions demands a careful implementation of seismic protection and conservation strategies. In this respect, motion-control techniques are crucial to safeguard monumental structures against deterioration or collapse during strong ground motion. Although the detailed numerical modelling of historical buildings is difficulted by uncertainties in the estimation of material and member characteristics,[1] the dynamic response of many monuments and structures made of large stone blocks can be characterized by the rocking behaviour of a rigid body.[2-4] The strong nonlinearities experienced by a rocking structure[5] and the challenges associted with modelling impact phenomena[6] prevent a precise estimation of its rotational response under a given base motion.[7] Neverthless, the classical rocking model proposed by Housner[8] has been shown able to predict the main statistics of the seismic response of rocking structures with reasonable accuracy.[9]

Much past research has been devoted to the prediction of the response of rocking structures subjected to various kinds of base motion, including harmonic pulses,[10,11] earthquake action,[12,13] and random excitation.[14] By contrast, studies on control strategies applicable to rocking bodies are limited and have been generally concerned with the protection of equipment or art objects.[15] Some of the proposed interventions involve lowering the centre of mass of the structure or suppressing its rocking motion all together by fixing it to a rigid base.[16] Such measures are intrusive in nature and can lead to unintended stress concentrations and damage during earthquakes. Similarly, a number of researchers have studied the use of appendages and devices attached to the rocking body to modify its seismic response. For example, De Leo et al[17] analysed the behaviour of a rocking structure with a pendulum attached to it acting as a vibration absorber. They observed important improvements in the overturning capacity of blocks with pendulums in comparison with uncontrolled structures. Nevertheless, the strong nonlinearities of the system made the design of the pendulum extremely difficult and potentially inefficient. In an effort to reduce the influence of nonlinarities, Simoneschi et al[18] studied the response of a block equipped with a tuned mass damper with linear visco-elastic properties attached at its top. Reasonable results were reported and the frequency ranges over which the use of the mass damper is not effective were identified. Other studies examined the potential of sloshing dampers to mitigate rocking.[19] Similarly, after studying the stability of rocking blocks standing on seismically isolated bases, Vassiliou and Makris[20] concluded that seismic isolation is only beneficial for small structures. More recently, Thiers-Moggia and Málaga-Chuquitaype[21] have explored the seismic control potential of inerters, which are mechanical devices that output forces proportional to the relative acceleration between their terminals. They demonstrated that supplemental rotational inertia devices effectively reduce the frequency parameter of rocking blocks, resulting in lower seismic rotation demands and enhanced stability due to the well-known size effects of the rocking behaviour.

In terms of remote options, a new device for the seismic protection of building clusters, designated as vibrating barrier (ViBa), has been recently proposed by Cacciola and Tombari.[22] It consists of a buried oscillator, detached from the surrounding structures and tuned to act as a vibration absorber. By using linearized approximations, Cacciola and Tombari[22] showed that a well-designed ViBa can mitigate the ground-motion effects on a building cluster where each structure is idealized as an elastic single degree of freedom system. On the other hand, their study also highlighted the need of a sizeable supplemental mass (comparable with the mass of the structures to be protected) as a major drawback of the ViBa. This handicap was further analysed by Cacciola et al[23] who explored the use of an inerter coupled with the ViBa in order to reduce the mass demands of the damper. As before, linear discrete approximations of soil and buildings were employed and the lateral displacement of the elastic building oscillator was used as the response parameter.

The concept of using external resonators as a means of vibration absorption is revisited in this paper and applied to the seismic protection of historical structures exhibiting highly nonlinear rocking behaviour. Figure 1 presents a schematic view of such an intervention where the structure is represented by a rocking block on a relatively rigid foundation. External resonators, contained within their respective foundation boxes, are buried in the adjacent soil and used as vibration absorbers. The resonators can be coupled with inerters in order to achieve large values of inertial mass from relatively minor quantities of gravitational mass.

We contend that the true potential of external resonators lies in their application to the seismic protection of monuments and historical structures where the space, strength, and architectural constrains favour the use of nonlocal control

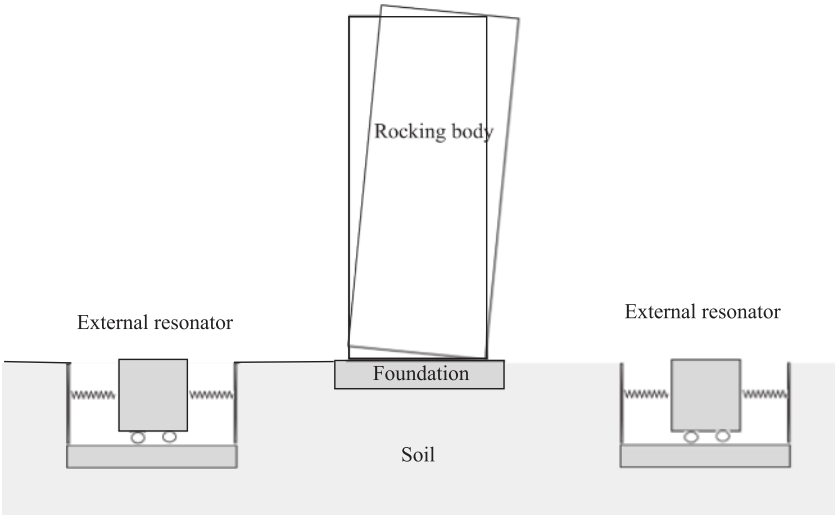

FIGURE 1 Seismic vibration control of a rocking body. Concept

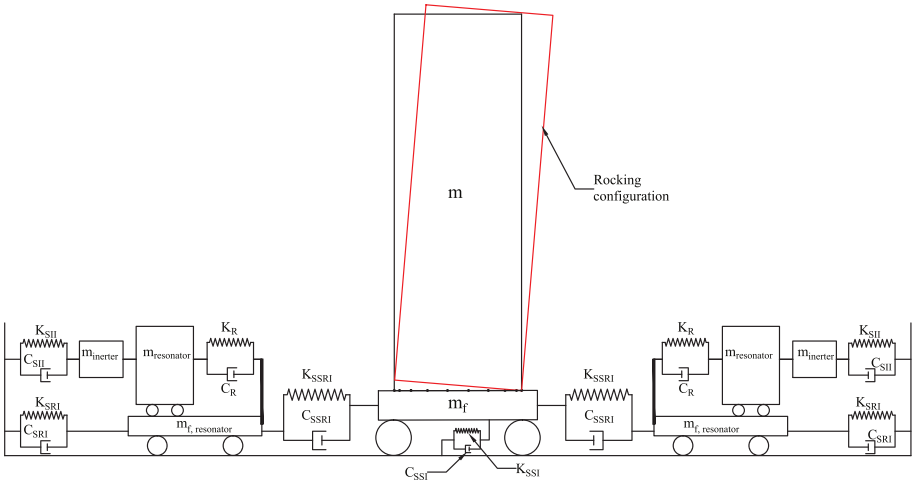

FIGURE 2 Seismic vibration control of a rocking body through external resonators and inerter devices. Schematic view of the discrete model idealization [Colour figure can be viewed at wileyonlinelibrary.com]

strategies and where rocking is the main mode of motion. However, this is not a minor development and several hurdles need to be carefully addressed in order to prove this concept. In the first place, the highly nonlinear nature of the rocking motion with its amplitude-dependent frequency of oscillation[8] configures a drastic departure from previous studies on linear-elastic structures. Furthermore, the competition between size and slenderness[24] makes the rotational response and overturning of a rocking body highly sensitive to the predominant frequency of the main energetic pulse of the excitation and to its structural configuration. To this end, in this study, we perform an extensive parametric study on discrete finite-element (FE) models involving rocking blocks of different slenderness subjected to coherent pulses of varying intensity. The influence of key parameters, such as the block slenderness, the mass, stiffness, and damping of the resonator, and the stiffness and damping of the soil and the soil-structure-resonator system, is examined. The results reveal the existence of a threshold frequency ratio above which the use of external resonators becomes ineffective. Finally, we conduct a detailed assessment of rocking demands using a set of real pulse-like ground motion records. We demonstrate that the use of external resonators is an attractive alternative to control peak seismic rotational demands of rocking structures and that the incorporation of the inerter effectively reduces the requirements for supplemental mass in the device up to a certain extent although its ability to mitigate structural overturning is restrained to particular frequency ranges.

2 | NUMERICAL MODELS

To conduct the series of analyses presented in this paper, discrete mechanical FE models of the structure-soil-resonator system proposed (Figure 1) were constructed in the finite element framework OpenSees.[25] A schematic representation of the mechanical components of one of such models is shown in Figure 2. Each model comprises of a stiff rocking structure flanked by two symmetric external resonating devices. In Figure 2, m stands for the mass of the rocking structure, m_f is the mass of its foundation, K_{SSRI} and C_{SSRI} are the stiffness and damping coefficient of the soil-structure-resonator approximations, respectively, $m_{resonator}$, K_R and C_R are the mass, stiffness, and damping coefficient of the external resonator, K_{SRI} and C_{SRI} are the stiffness and damping coefficient used to simulate the soil-resonator interaction, and K_{SSI} and C_{SSI} are the stiffness and damping coefficient used to simulate the soil-structure interaction. Besides, $m_{inerter}$ represents the supplemental inertial mass brought about by the inerter, if such device is present. If no inerter is provided, the $m_{resonator}$ is connected on one side only to its foundation box through K_R and C_R. If a grounded inerter is employed, the connection between the inerter and the ground is characterized by means of its stiffess, K_{SII}, and damping coefficient, C_{SII}.

To facilitate the proof of concept and subsequent comparisons, we consider a unidirectional motion within a 2D structural representation. It is acknowledged that this representation is particularly suitable to rigid blocks of rectangular base with one side considerably larger than the other. However, the general trends identified in our study are a first-level approximation and are expected to remain relevant for multidirectional actions where, if needed, an array of distinctly oriented resonators can be used to control a 3D rocking motion.

2.1 | Rocking structure

In general, the modelling principles proposed by Vassiliou et al[26] are followed herein to simulate the superstructure and its rocking interface as depicted in Figure 3. To this effect, the rocking interface between the superstructure and its support

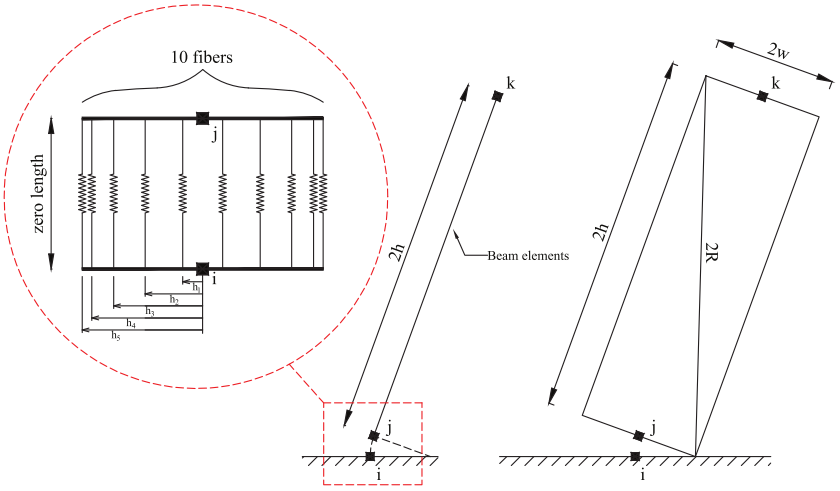

FIGURE 3 Finite-element model of the rocking structure. After Vassiliou et al[26] and Spieth et al[28]

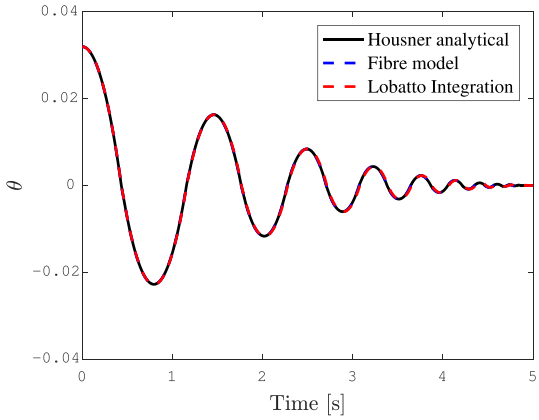

FIGURE 4 Comparison of analytical and numerical rotation histories

can be modelled via zero-length elements with elastic-no-tension resistance and a relatively large compression modulus of elasticity. No viscous damping is employed for the rocking body, as suggested by Vassiliou et al,[26] instead numerical damping through the Hilber-Hughes-Taylor (HHT) algorithm[27] is used to simulate the energy dissipation at the impact between the rocking body and its foundation. The rocking body is modelled via elastic-beam-column elements. Recalling that the moment of inertia of a rigid rectangular block rocking about its pivot corner is $4/3mR^2$ whereas the moment of inertia of a beam-column element with translational masses is $1/3mR^2\cos^2\alpha + mR^2$, where α is the slenderness of the block ($\alpha = \arctan b/h$), the difference, $1/3mR^2\sin^2\alpha$, is assigned to the rotational degrees of freedom of the nodes along the height of the rocking building.[26]

Figure 4 shows an example of a comparison between Housner's analytical prediction and the numerical estimations obtained as described above. The plots correspond to the rotational response of a rectangular block undergoing free rocking motion after being pushed to a tilted position. Preliminary sensitivity studies were carried out as part of the present study to assess the influence of the number of elements and HHT dissipation factor. To this end, 20 beam-column elements were used to represent the rocking body and a HHT dissipation factor of 0.90 was employed. The response of the whole system was not found to be sensitive to reasonable variations of this factor.

When a rigid block rocking on a rigid foundation is considered, only two springs, one at each corner, are enough to simulate its response. However, in order to incorporate the characteristics of a flexible foundation, a simplified multi-spring approach was followed as also presented in Figure 3. To this end, the spring location and their relative stiffnesses were calculated using the Lobatto integration scheme introduced by Spieth et al[28] starting from the global vertical stiffness of the foundation determined as described in Richart and Whitman.[29] This approach allows for a realistic modelling of the contact compression zones and the relocation of the pivot point due to local flexibility, if necessary. Previous studies have demonstrated that the number of gap elements along a rocking surface can be calculated by dividing its length by a factor of 10.[30] Alternatively, each zero-length spring in Figure 3 can be defined via a fibre section (as in the original proposal by Vassiliou et al[26]) with the cross-sectional area of each fibre following the Lobatto distribution mentioned above.

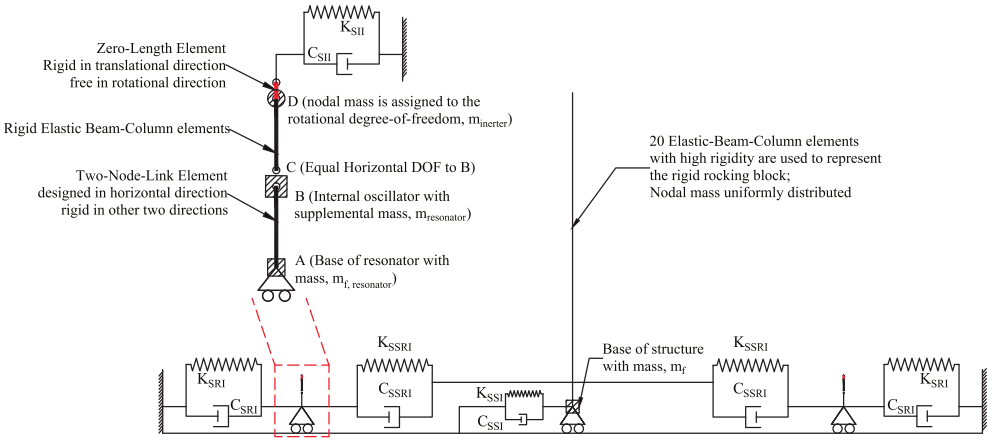

FIGURE 5 Finite-element model of the soil-structure, soil-resonator, and soil-structure-resonator system [Colour figure can be viewed at wileyonlinelibrary.com]

2.2 | Soil-structure, soil-resonator, and soil-structure-resonator interactions

Simplified discrete based models were employed to represent the soil-structure interaction (SSI), soil-resonator interaction (SRI), and soil-structure-resonator interaction (SSRI). This modelling approach is based on the principles described and verified in the available scientific literature.[31-35] Such models have been found to capture well the interactions between resonators and soil when this latter is simulated by means of more comprehensive continuum models.[22] Figure 5 illustrates the FE components employed. The external resonators are approximated via two-node-link elements while the SSI, SRI, and SSRI are simulated via visco-elastic truss elements.

2.2.1 | SSI and SRI

The same expressions were employed to estimate the SSI and SRI parameters.[31,32] To this end, the horizontal (K_h) and vertical (K_v) stiffness of the discrete truss element employed to model these interactions were defined as follows:

$$K_h = \frac{8GR_0}{2-\nu} J_h \left(\frac{L}{B}\right), \quad K_v = \frac{4GR_0}{1-\nu} J_v \left(\frac{L}{B}\right), \tag{1}$$

where G is the shear modulus of the soil, ν is the Poisson's ratio, L and B are the dimensions of the foundation of the structure or resonator, and J_h is a correction factor calibrated by Gazetas.[32] Additionally, the corresponding damping coefficients can be approximated by the following:

$$\xi_h = \frac{0.29}{\bar{m}_h^{1/2}}, \quad \xi_v = \frac{0.425}{\bar{m}_v^{1/2}}, \tag{2}$$

with

$$\bar{m_h} = \frac{m(2-\nu)}{8\rho R^3}, \quad \bar{m_v} = \frac{m(1-\nu)}{4\rho R^3}, \tag{3}$$

where m is the mass of foundation of the rocking block or resonators, ν is the Poisson's ratio of the soil, ρ is the mass density of the soil, and R is the equivalent circular radius of the foundation. Similarly, the damping coefficient C_{SSI} can be obtained from the damping ratio (ξ) as $C_{SSI} = 2\xi\sqrt{KM}$ where K and ξ are defined in equations 1 and 2 and M is the mass of the foundation. The employed idealizations approximate radiation and hysteretic damping and consider basic kinematic interactions but the rotational motion of the foundation is disregarded. This latter assumption is not considered determinant for the dimensionless comparisons that follow which are consistently performed in relative terms. Likewise, approximate impedance factors are applied as recommended in previous studies[29,32] and used in Vassiliou et al,[31] among others, to incorporate the dynamic effects on the SSI, SRI, and SSRI.

2.2.2 | SSRI

In order to account for SSRI effects, the coupling between the two foundations is simulated via discrete stiffness and damping elements whose stiffness and damping can be approximated by[33] the following:

$$K_{SSRI} = \Gamma \frac{Ga}{2-\nu}, \tag{4}$$

$$C_{SSRI} = \Psi \frac{Ga^2}{V_s(2-\nu)}, \tag{5}$$

where $\Gamma = 3.7561 \cdot 10^{-0.18995(d/a)}$ and $\Psi = 13.2875$, with d being the distance between the two foundations and a the foundation dimensions, respectively.

It is worth noting that the stiffness and damping of an elastic media are frequency-dependent.[36] However, the parametric studies undertaken herein to prove the concept cover a reasonable range of soil parameters that encompass the frequency amplification effects[36] most commonly expected in practice.

2.3 | Inerter

In this paper, we also evaluate the use of supplemental rotational inertia devices, or inerters, acting in combination with the external resonators. The supplemental inertia provided by these devices is intended to alleviate the need for very large supplemental masses on the vibration absorbers, which can reach magnitudes comparable to the mass of the protected structure. An inerter is a mechanical element which output force is proportional to the relative acceleration between its terminals[37,38] and which constant of proportionality is called inertance. Previous work[39,40] has shown that inerters can generate inertial forces several orders of magnitude higher than those corresponding to the gravitational mass deployed. In this respect, resonators equipped with inerters can be used to alleviate the need for large supplemental masses which can sometimes reach magnitudes comparable with the mass of the protected structure.

The inerter considered in this study corresponds to a rack-and-pinion flywheel system and its numerical implementation in OpenSees follows the proposal of Málaga-Chuquitaype et al[41] shown schematically in Figure 5. This FE representation of an inerter consists of two connected nodes with an angular mass assigned to the rotational degree of freedom of the master node. This node represents the pivot of a rotating flywheel, whereas the slave node corresponds to the pinion gear. The model transforms the horizontal relative displacement between the terminals into a rotation in the flywheel node.

It is evident that the contribution of the inerter to the dynamic response of the system depicted in Figure 2 is a function of its apparent mass and the relative acceleration between the resonator mass, $m_{resonator}$, and the grounded terminal of the inerter. This latter, in turn, will depend on the characteristics of the anchoring employed which will define the values of K_{SII} and C_{SII} (Figure 5). In order to simplify the analyses that follow, a perfectly rigid connection (i.e., $K_{SII} \approx \infty$) is assumed throughout this study. It is recognised that this is an upper bound case, which can nevertheless be approximated by a careful design of the interter-ground connection that minimizes its compliance. On the other hand, the apparent mass of the inerter can be increased by employing a gearing system[38] that amplifies the rotational motion of the device. These different levels of rotation amplification are accounted for by changing the distance between nodes C and D in the model (Figure 5).

3 | ROCKING DEMANDS UNDER PULSE-TYPE EXCITATIONS

This section presents a first assessment of the benefits of employing external resonators for the control of rocking demands in rigid blocks. This evaluation was carried out by subjecting a range of FE models, constructed as described in the previous section, to coherent acceleration pulses of varying intensity. To this end, Mavroeidis and Papageorgiou (MP) velocity pulses[42] with varying amplitudes, A_p, and frequency parameters, f_p, were employed. The analytical expressions developed in MP[42] for representing the ground velocity and the corresponding acceleration histories of ideal near-field pulse-like ground motions are presented in Equations 6 and 7, respectively, as follows:

$$\dot{u}_g(t) = \frac{A_p}{2}\left[1+\cos\left(\frac{2\pi f_p}{g_p}(t-t_0)\right)\right]\cos\left[2\pi f_p(t-t_0)+\eta\right] \quad t_0 - \frac{g_p}{2f_p} \le t \le t_0 + \frac{g_p}{2f_p}, \tag{6}$$

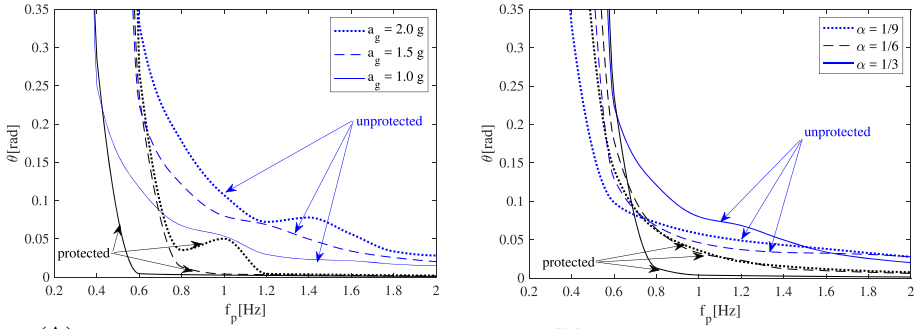

(A) Influence of the intensity of the ground-motion. $\alpha = 1/3$.

(B) Influence of the block slenderness. $a_g = 1.5g$

FIGURE 6 Example of rocking demands for protected and unprotected rocking structures

$$\ddot{u}_g(t) = \frac{A_p \pi f_p}{g_p} \left\{ \begin{array}{l} \sin\left(\frac{2\pi f_p}{g_p}(t-t_0)\right) \cos\left(2\pi f_p(t-t_0) - \pi g_p + \eta\right) \\ \quad - g_p \sin\left(2\pi f_p(t-t_0) - \pi g_p + \eta\right) \left[1 - \cos\left(\frac{2\pi f_p}{g_p}(t-t_0)\right)\right] \end{array} \right\} t_0 - \frac{g_p}{2f_p} \le t \le t_0 + \frac{g_p}{2f_p}. \quad (7)$$

In these equations, the parameter A_p defines the velocity-pulse amplitude, η is the phase angle of the harmonic excitation which is assumed to be 0 throughout this study, $f_p (= 1/T_p)$ is the prevailing frequency of the pulse, g_p determines the oscillatory character of the pulse, and t_0 defines the peak of the of the excitation envelope. An important feature of the MP model is the relationship between the pulse duration and the input parameters (i.e., pulse duration equals g_p/f_p). Likewise, the prevailing frequency is related to the magnitude, M_w, of the ground motion by[42] the following:

$$\log(1/f_p) = -2.9 + 0.5M_W. \quad (8)$$

The relative simplicity of equations 6 and 7, together with the physically realizable nature of the motions, makes MP pulses a neat tool for parametric studies.[43,44]

Figure 6 offers a clear assessment of the benefits of employing external resonators. It compares the rocking spectra of protected and unprotected structures, where protected stands for systems that incorporate external resonating devices. It is apparent from Figure 6A that employing external resonators brings significant benefits to the rocking response. These benefits are noticeable for all intensities of ground motion when $\alpha = 1/3$ (Figure 6A). For less slender blocks (e.g., $\alpha < 1/6$) under a intensity of PGA = 1.5 g, the rocking demand can still be reduced by the resonators in the high-frequency range (e.g., $f_p > 0.7$ Hz) although the reduction is less appreciable than in stocky blocks. In general, for a given system (i.e., $m_{resonator} = 0.5m$, $K_R = 2 \times 10^4$ N/m, $K_{SSI} = 4.61 \times 10^5$ N/m, $K_{SSRI} = 4.96 \times 10^5$ N/m, $K_{SRI} = 2.31 \times 10^5$ N/m, $\xi_{SSI} = 1.5\%$, $\xi_{SSRI} = 1.7\%$, $\xi_{SRI} = 1.5\%$ and $\xi_R = 1.0\%$ in the case of Figure 6) a threshold frequency ratio can be identified below which the effects of the external resonator will be detrimental. The precise location of such frequency thresholds can be altered depending on the design of the external resonators, as will be discussed latter in this paper. Importantly, on the spectral regions where the resonating devices are effective, very significant reductions in rocking demands are observed, with peak rotations in controlled structures reaching a 75% reduction or more in rotation magnitudes at frequency ratios close to overturning.

4 | PARAMETRIC ANALYSES

We conducted a parametric investigation on the response of rocking structures with external resonating devices under coherent MP pulses in order to understand the influence of the mass and stiffness of the resonator, its damping, and the SSI parameters. The parameters selected were varied over a carefully selected range in order to reflect the characteristics of physically realizable configurations. The results of the parametric studies are summarized in Figures 6 to 12 and will be discussed in detail in the following sections.

4.1 | Dimensional analysis and parameter space

The parameters governing the response of the system formed by the rocking block, its foundation, the soil, and the external resonators depicted in Figure 5 when subjected to a ground motion of frequency f_p and amplitude a_g are: the response

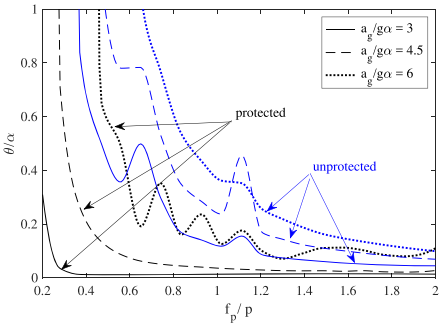

(A) Influence of the intensity of the ground-motion. $\alpha = 1/3$.

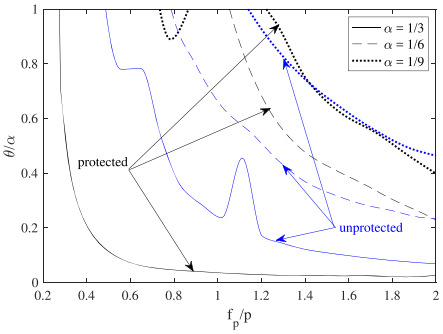

(B) Influence of the block slenderness. $a_g = 1.5g$

FIGURE 7 Comparison of dimensionless rocking spectra

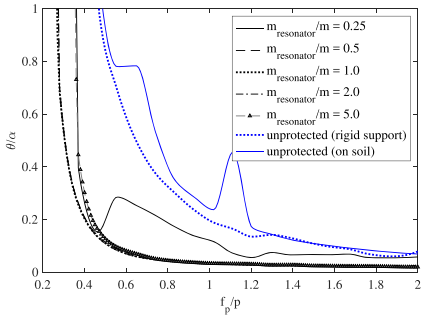

(A) $\alpha = 1/3$.

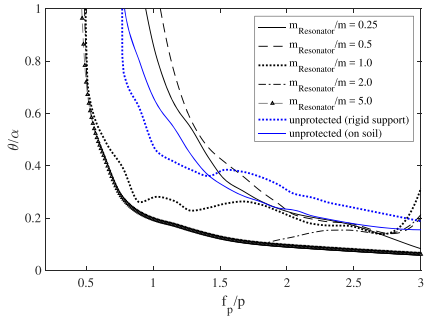

(B) $\alpha = 1/6$.

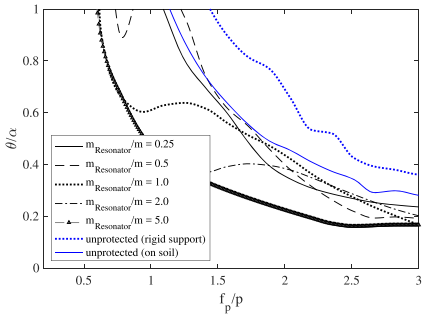

(C) $\alpha = 1/9$.

FIGURE 8 Influence of the mass of the resonator, $m_{resonator}$. Unprotected refers to systems without external resonators

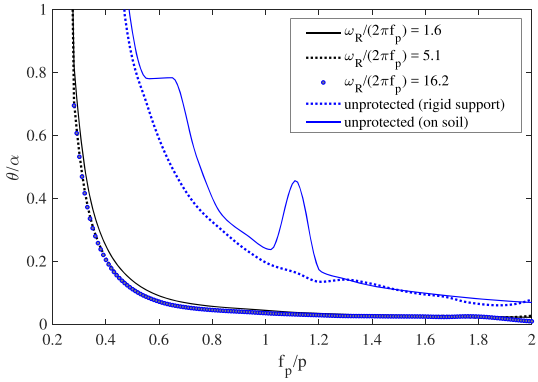

FIGURE 9 Influence of the stiffness of the resonators, K_R. Unprotected refers to systems without external resonators

quantity of interest, which in this case is the maximum rotation of the rigid block (θ); the block slenderness (α); its frequency parameter (p) and mass (m); the mass of the foundation (m_f); the mass of the resonator ($m_{resonator}$), its stiffness (K_R) and damping (C_R); the mass of the resonator foundation ($m_{f,resonator}$); and the stiffness and damping corresponding to the soil-structure (K_{SSI}, C_{SSI}), soil-resonator (K_{SRI}, C_{SRI}), and soil-structure-resonator (K_{SSRI}, C_{SSRI}) interaction parameters, the apparent mass of the inerter ($m_{inerter}$), the inerter-ground connection stiffness and damping (K_{SII}, C_{SII}), as well as the ground motion parameters (a_g, f_p):

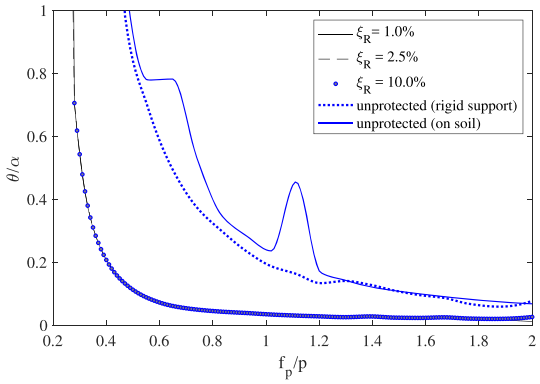

FIGURE 10 Influence of the resonators damping. Unprotected refers to systems without external resonators

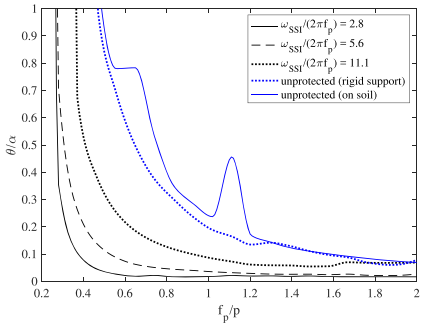

(A) Influence of the soil-structure interaction stiffness, K_{SSI}.

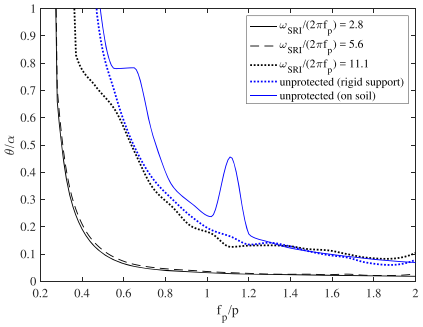

(B) Influence of the soil-resonator interaction stiffness, K_{SRI}.

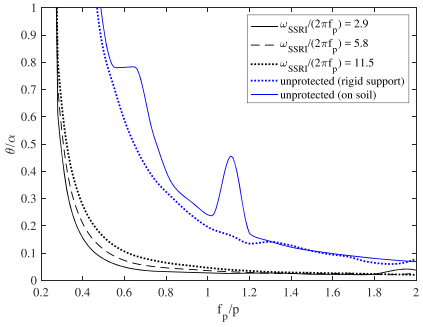

(C) Influence of the structure-soil-resonator interaction stiffness, K_{SSRI}.

FIGURE 11 Influence of the soil interaction stiffness. Unprotected refers to systems without external resonators

$$\theta = f\left(\alpha, p, m, m_f, m_{resonator}, m_{f,\,resonator}, m_{inerter}, K_R, C_R, K_{SSI}, C_{SSI}, K_{SRI}, C_{SRI}, K_{SSRI}, C_{SSRI}, K_{SII}, C_{SII}, a_g, f_p, g\right). \quad (9)$$

This results in a group of 21 characteristic variables involving three reference dimensions, those of length [L], time [T], and mass [M]. As mentioned above, a rigid inerter-ground connection is assumed herein (i.e., $K_{SII} \approx \infty$, $C_{SII} \approx 0$) together with a constant fundation to superstructure ratio (i.e., $m_f/m = m_{f,resonator}/m_{resonator} = 0.10$). Therefore, the application of Vaschy-Buckingham's Π-theorem[45,46] to this newly constrained variable space leads to the following 14 independent dimensionless Π-products:

$$\theta = \phi\left(\alpha, \frac{f_p}{p}, \frac{m_{resonator}}{m}, \frac{m_{inerter}}{m}, \frac{\omega_R}{2\pi f_p}, \xi_R, \frac{\omega_{SSI}}{2\pi f_p}, \xi_{SSI}, \frac{\omega_{SRI}}{2\pi f_p}, \xi_{SRI}, \frac{\omega_{SSRI}}{2\pi f_p}, \xi_{SSRI}, \frac{a_g}{g}\right), \quad (10)$$

where

$$\omega_R = \sqrt{\frac{K_R}{m_{resonator}}}, \quad \omega_{SSI} = \sqrt{\frac{K_{SSI}}{m_f}}, \quad \omega_{SRI} = \sqrt{\frac{K_{SRI}}{m_{f,\quad resonator}}}, \quad \omega_{SSRI} = \sqrt{\frac{K_{SSRI}}{m_f}} \quad (11)$$

$$\xi_R = \frac{C_R}{2\left(m_{resonator} + m_{inerter}\right)\omega_R}, \quad \xi_{SSI} = \frac{C_{SSI}}{2m_f\omega_{SSI}}, \quad \xi_{SRI} = \frac{C_{SRI}}{2m_{f,\quad resonator}\omega_{SRI}}, \quad \xi_{SSRI} = \frac{C_{SSRI}}{2m_f\omega_{SSRI}}. \quad (12)$$

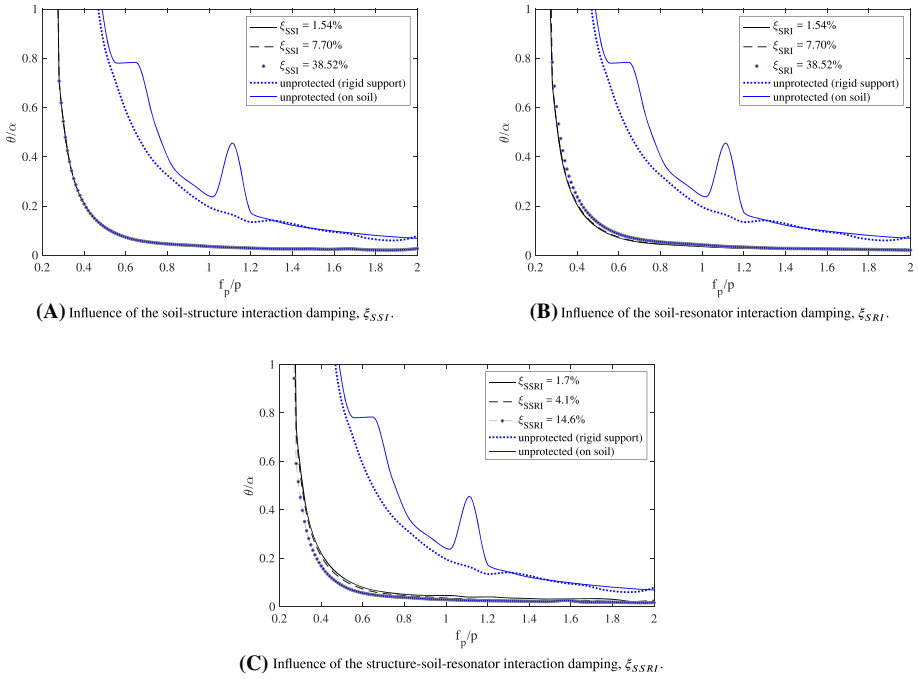

(A) Influence of the soil-structure interaction damping, ξ_{SSI}.

(B) Influence of the soil-resonator interaction damping, ξ_{SRI}.

(C) Influence of the structure-soil-resonator interaction damping, ξ_{SSRI}.

FIGURE 12 Influence of the soil interaction damping. Unprotected refers to systems without external resonators

TABLE 1 Summary of range of variation of dimensionless parameters

	$\frac{a_g}{g}$	$\frac{f_p}{p}$	$\frac{\omega_R}{2\pi f_p}$	ξ_R	$\frac{\omega_{SSI}}{2\pi f_p}$	ξ_{SSI}	$\frac{\omega_{SRI}}{2\pi f_p}$	ξ_{SRI}	$\frac{\omega_{SSRI}}{2\pi f_p}$	ξ_{SSRI}	$\frac{m_{resonator}}{m}$	$\frac{m_{inerter}}{m}$	α
Min	1.0	0.1	1.62	0.01	2.8	0.015	2.8	0.015	2.9	0.017	0.25	0.0	1/9
Max	2.0	2.0	16.24	0.10	11.1	0.38	11.1	0.38	11.5	0.15	5	4.0	1/3
Base case	1.5	Variable	5.14	0.025	5.6	0.077	5.6	0.077	5.8	0.041	0.5	0.5	1/3

In the analyses that follow, the influence of a given parameter is assessed by changing its value between predefined ranges while keeping all other parameters constant. This involves the generation of a series of consistently dimensionless systems since many of the Π products of Equation (10) are dependent on f_p.

Importantly, the ranges for the variation of the dimensionless parameters were selected to broadly represent realistic configurations. These ranges are summarized in Table 1 together with the base case scenario employed as a control point. In general, 4-m wide rocking structures with aspect ratios between 1/3 and 1/9 were analysed. These configurations are broadly consistent with a range of historical structures and buildings.[47,48] The horizontal distance between the rocking block and the resonator was typically 10 m with a 2 by 2 m foundation box. Finally, comparisons are also established against the response of the corresponding rocking block sitting on an ideal rigid foundation and the response of an unprotected rocking body resting on a soil corresponding to the base case (i.e., assuming the *R*, *SRI*, and *SSRI* terms equal to zero).

Figure 7 presents and compares dimensionless rocking spectra of protected and unprotected structures. The parameters of these analyses correspond to the base case scenario in Table 1, except for the acceleration and block slenderness which are reported in the figure. The block peak rotations obtained from the response history analyses considering deformable soil conditions are depicted in this figure as a function of the frequency ratio, f_p/p, where f_p is the prevailing frequency of the ground motion and p is the rocking block frequency parameter[8] defined as $p = \sqrt{3g/4R}$. Results are presented for structures of different slenderness (α) and for various ground-motion intensities ($a_g/g\alpha$). In these graphs, rotations of $\theta/\alpha > 1$ denote overturning. Zhang and Makris[10] have noted the existence of safe regions located above the minimum acceleration levels associated with overturning of rigid blocks on the acceleration-frequency plane. However, even if the rocking body survives the ground motion without overturning, the high rotations and angular accelerations that can be experienced during ground-shaking may be damaging to the structure; therefore, our attention was placed on θ/α rotations equal to or less than 1.

The influence of external resonators can be assessed by comparing the rocking spectra of protected and unprotected structures depicted in Figure 7 where protected stands for systems that incorporate external resonating devices. In general, the protected structures experience lower rocking demand across all the frequency range considered under all

intensities of ground motion. In addition, it is apparent from Figure 7A that the benefits of employing external resonators are greater for lower intensities of ground motion although the reduction in peak rotations still reaches 50% across the wide spectral region under highest intensity.

Figure 7B shows the influence of aspect ratios on the rocking demand. The resonators can alleviate the rocking amplitude over the entire spectral region in the case of $\alpha = 1/3$. However, as the structure becomes slenderer, a threshold frequency ratio, f_p/p_{lim}, can be identified below which the effects of external resonators will be detrimental. This frequency limit is relatively large for $\alpha = 1/6$ in Figure 7B where a resonator mass of $m_{resonator} = 0.5m$ is employed hinting to the need of larger masses as will be discussed in the parametric section of this paper. It is also worth noting that the seismic rotations in controlled structures present a sharp increase in the proximity of the frequency ratio threshold, f_p/p_{lim}, while they remain very close to zero for higher frequencies (shorter pulses). Besides, the rotational demands of structures with resonators are less sensitive to the pulse intensity or the block slenderness in the high frequency region of the spectra.

4.2 | Resonator mass

Figure 8 provides an insight on the evolution of the rocking response of structures with external resonators of different masses. The cases presented correspond to a ground motion intensity of $a_g/g\alpha = 4.5$, rocking blocks of $\alpha = 1/3$, 1/6 and 1/9, $\omega_R/2\pi f_p = 5.14$, and $\omega_{SSRI}/2\pi f_p = 5.8$. Five different levels of supplemental mass are explored in Figure 8, namely $m_{resonator} = \{0.25m, 0.5m, 1.0m, 2.0m, 5.0m\}$. An inerter with an apparent mass or inertance of $m_{inerter} = 0.5m$ is used in all cases. The rocking spectra for an unprotected structure of the same characteristics resting on deformable soil (base case without resonator) and on an ideally rigid medium are also included in Figure 8 for comparison. A marked decrease in rotation demands of structures with resonators is observed for all ranges of f_p/p when $\alpha = 1/3$. This reduction in seismic demands is particularly noticeable at frequency ratios of $f_p/p > 0.4$ in Figure 8A for $\alpha = 1/3$. It is also evident from this figure that a large external mass, in the order of $m_{resonator} = m$, leads to a better mitigation of the amplitude of rocking motion extending the range of efficiency of the resonators towards proportionally lower frequencies. This mass increment also leads to a noticeable increase in the block overturning capacity in comparison with the original structure. However, resonator masses above the $m_{resonator} = m$ level become progressively less effective in the short frequency range $0.28 < f_p/p < 0.6$ with very large resonator masses (e.g., $m_{resonator} = 4m$) being less able to control rocking than the mresonator = 0.25 m case at short frequency ratios.

The need for larger resonator masses to control the response of more slender blocks is verified in Figure 8B,C for blocks of slendernesses $\alpha = 1/6$ and $\alpha = 1/9$, respectively. In the case of $\alpha = 1/6$ structures, the existence of a region (e.g., $f_p/p < 2$) where the use of external resonators is detrimental to the seismic response is evidenced. In these cases, low resonator masses (i.e., $m_{resonator} = 0.25$ or 0.5 m) are associated with higher vulnerabilities to overturning and larger masses in the order of $m_{resonator} = m$ or larger are required to shift the frequency ratio linked to overturning towards lower levels. Similar trends are observed for blocks with $\alpha = 1/9$ (Figure 8C) where $m_{resonator} = 0.25$ or 0.5 m do not lead to significant improvements in the response. As stated above, the requirement for a large tuned mass can be alleviated if inerter devices are employed to amplify the supplemental inertia of the vibrating block.

4.3 | Resonator stiffness

Figure 9 summarizes the effects of changing the stiffness of the resonator's spring (i.e., $\omega_R/2\pi f_p = 1.6, \omega_R/2\pi f_p = 5.1, \omega_R/2\pi f_p = 16.2$) for systems with $\alpha = 1/3$, $m_{resonator} = m$, and $\omega_{SSRI}/2\pi f_p = 5.8$. A ground motion intensity of $a_g/g\alpha = 4.5$ is employed. As before, the rocking spectra for an unprotected structure with comparable properties resting on deformable soil and on an ideally rigid foundation is also depicted in Figure 9 to facilitate the comparisons. It can be concluded from this figure that, provided the spring of the resonator is not low in comparison with the soil, the ability of the system to control rocking demands is not affected. More flexible resonators will lead to slightly higher rotational demands, as appreciated from Figure 9, but overall the reductions in peak rotations are significant. This should be understood in the context of the soil characteristics, as will be discussed later, with stiffer soils requiring stiffer resonating devices to transfer the required forces.

4.4 | Resonator damping

The influence of the energy loss in the resonator, accounted via viscous damping in our models, is explored in Figure 10. Three different values of viscous damping ratio are analysed including $\xi_R = 1\%$, $\xi_R = 2.5\%$, and $\xi_R = 10\%$ while the rest of the modelling parameters correspond to the base case in Table 1. A high damping value is considered to represent the

provision of a supplemental source of energy dissipation or a marked increase in the viscous coefficient associated with an inefficient mechanism or faulty design. Similarly, a value of $\xi_R = 1\%$ represents a lower bound of energy dissipation capacity. It can be seen from Figure 10 that these important variations in damping are virtually immaterial to the rocking response of the structure.

4.5 | Soil-structure interaction

The equivalent soil properties (stiffness and damping) can take a wide range of values covering several orders of magnitude across different soil types. This leads to a high variation of K_{SSRI}, K_{SRI}, C_{SSRI}, and C_{SRI} even if the foundations of the resonators and building remain unchanged. In order to identify general response tendencies, the soil stiffness was varied within the range proposed in Table 1. The approximations employed to define the SSI, SRI, and SSRI-related parameters have been discussed in detail in previous parts of this paper. In this section, it is our interest to examine the effects brought about by implementing external resonating devices in soils of broadly defined moderately stiff and soft categories. It should be noted that, although the soil stiffness and damping will be determined by the particular site conditions, there is important room for manoeuvre in the design of the resonators foundation that can be strategically dimensioned to provide desired levels of K_{SRI} and K_{SSRI} stiffness. To this end, Figure 11 presents the response of rocking structures with vibrating devices of the same characteristics in terms of mass and stiffness ($m_{resonator} = 0.5m$, $\omega_R/2\pi f_p = 5.14$) but placed on soils of different types and stiffness. Likewise, Figure 12 summarises the results for different levels of energy dissipation in the soil components characterized by different viscous damping coefficients. It can be concluded from these figures that external resonators located in more flexible soils are able to control better the rocking of the protected structure over a wider range of frequencies. Figure 11 shows that external resonators on flexible soils successfully suppress the rocking due to pulses with significantly low frequencies and that a reduction of the frequency associated with overturning, $f_p/p_{(\theta/\alpha=1)}$, is possible under these conditions. As the soil becomes stiffer, the resonators become less effective and can even amplify the response ($\omega_{SRI}/2\pi f_p = 11.1$ for $f_p/p > 1.25$ in Figure 11B). On the other hand, as noted above, levels of energy dissipation in the soil within realistic estimates do not influence significantly the ability of the resonator to control rocking as can be observed from Figure 12.

4.6 | External resonators with inerters

As discussed above, the coupling of an inerter with the external resonating mass can offer a potential solution for increasing the effective mass of the external resonator without increasing their gravitational mass. Previous research has shown that if amplifying mechanisms such as ball screws[49] or geared wheels[38] are used, high levels of inertial mass can be achieved keeping the associated gravitational mass at a minimum. To study this further, Figure 13 presents the rocking spectra for structures protected via external resonators whose masses have been connected to grounded inerters of various apparent mass levels. In all cases, the resonator has a mass $m_{resonator} = 0.5m$, and the soil media leads to $\omega_{SSI}/2\pi f_p = 5.6$, $\omega_{SRI}/2\pi f_p = 5.6$, $\omega_{SSRI}/2\pi f_p = 5.8$, and $\xi_{SSI} = 7\%$, $\xi_{SRI} = 7\%$, $\xi_{SSRI} = 4\%$. The rocking demands on the original unprotected structure on deformable and ideally rigid soils are also presented in Figure 13 for completeness.

In general, Figure 13 supports the concept of employing external coupled inerter-resonator systems for mitigating rocking. Significant response improvements are achieved by incorporating inerters when the mass of the resonator is relatively low in comparison with the mass of the rocking body. However, a maximum level of response control is obtained for an inertance of $m_{inerter}/m = 0.25$ in the case of $\alpha = 1/3$ (Figure 13A) while larger inertances lead to progressively larger peak rotations. This points to the existence of an optimal ($m_{resonator}$, $m_{inerter}$) pair beyond which the potential benefits of the external resonator are offset by the large forces and interactions brought about by the inerter. This, sometimes counter-productive, behaviour can induce potentially higher peak rotations similar to those in systems without inerters ($m_{inerter}/m = 0$). Such is the case when $m_{inerter}/m = 4$ for the frequency range $0.38 < f_p/p < 0.58$ in Figure 13A. In the case of more slender rocking blocks ($\alpha = 1/6$ and $\alpha = 1/9$ in Figures 13B,C), only the larger inertances (i.e., $m_{inerter}/m > 2$) are able to produce noticeable reductions in peak rotations with $m_{inerter} = 2m$ being associated with the higher demand reductions than $m_{inerter} = 4m$, which can be attributed to the larger forces generated by the device that need to be transferred to the soil-foundation system.

5 | RESPONSE UNDER REAL PULSE-LIKE GROUND MOTIONS

Previous sections have evaluated the benefits of employing external resonators, with and without inerters, for the control of rocking demands in structures utilizing ideally coherent MP pulses. This has facilitated a generic exploration of the

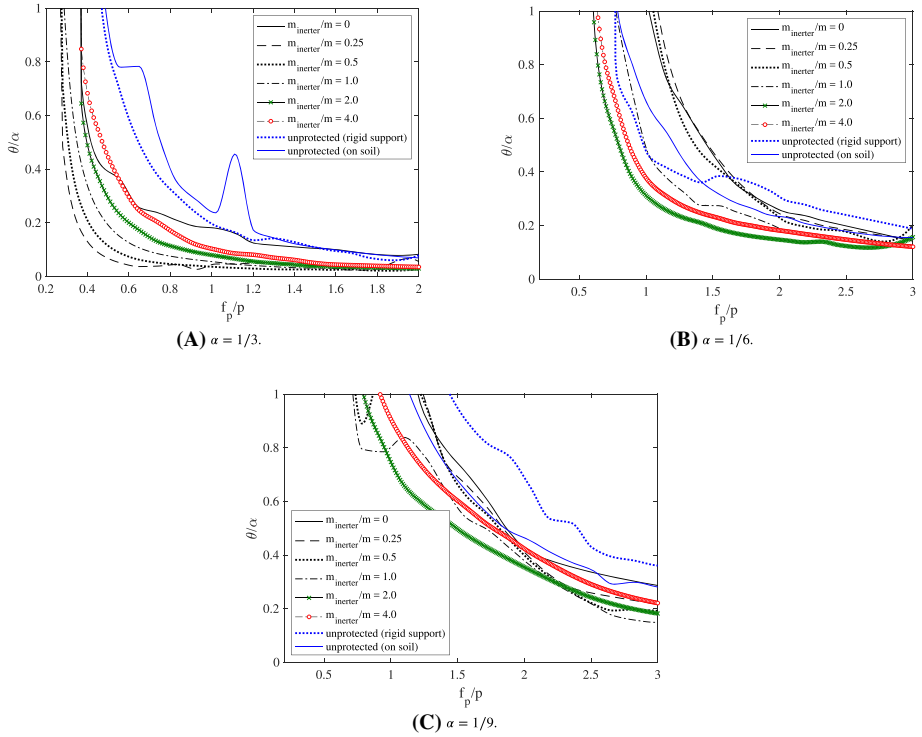

(A) $\alpha = 1/3$. **(B)** $\alpha = 1/6$. **(C)** $\alpha = 1/9$.

FIGURE 13 Influence of the inertance. Unprotected refers to systems without external resonators

influence of key parameters on the efficiency of the newly proposed control strategy. Nevertheless, real ground motions have a richer (noncoherent) spectral content that can potentially alter the seismic demands of rocking structures. In this section, we assess the response of rocking bodies with external resonating devices under a set of 42 real pulse-like acceleration series through detailed statistical comparisons. The selection of modelling parameters of the rocking block and soil-resonator system employed in this section is identical to that adopted in Figure 6 (Section 3).

5.1 | Record database and intensity measures

A set of real records with pulse-like features were employed to study the realistic behaviour of rocking structures equipped with external resonators. The set of records was obtained from the Pacific Earthquake Engineering Research Center (PEER) database and involves 21 earthquakes with magnitudes M_w ranging from 5.4 to 7.1. Table 2 summarizes the catalogue of earthquakes used in the analyses presented in this section. The range of ground-motion main pulse periods varies between 0.5 and 2 s. All accelerograms were scaled to attain a PGA of 1.5 g ($a_g/g\alpha = 4.5$). Besides, Dimitrakopoulos et al[50] demonstrated that intensity parameters defined in terms of the uniform duration t_{uni}, defined as the sum of the time intervals during which the ground acceleration exceeds the acceleration limit associated with uplifting, exhibit the greatest efficiency among different alternatives for quantifying rotational demands in rocking structures. For this reason, the proposed dimensionless parameter, pt_{uni}, is considered in the analyses that follow.

5.2 | Case study results and statistical analysis

A series of dynamic response history analyses were carried out by subjecting rocking structures with and without external resonators to the pulse-like ground-motion record set detailed above. In particular, the response of a system with the following characteristics is evaluated: $K_R = 2\times10^4$ N/m, $K_{SSI} = 4.61\times10^5$ N/m, $K_{SSRI} = 4.96\times10^5$ N/m, $K_{SRI} = 2.31\times10^5$ N/m, $\xi_{SSI} = 1.5\%$, $\xi_{SSRI} = 1.7\%$, $\xi_{SRI} = 1.5\%$, and $\xi_R = 1.0\%$. It comprises of a 4-m wide and 12-m tall rocking body with $\alpha = 18.5^o$ and resonators placed at a distance of 10 m from it. Both components of the earthquake were employed by applying them independently to the numerical models in their horizontal direction. The peak rotations were recorded and are presented in Figure 14. Cloud analyses were conducted on the database of results generated and used to assess the seismic rotation demands in protected and unprotected rocking structures. As before, the structural demands are described in terms of the dimensionless peak rotation θ/α and are now plotted in the θ/α-pt_{uni} logarithmic plane. Following standard practice, we consider a power law distribution for the median estimated demand, $\overline{D}_m$, as follows:

$$\overline{\theta/\alpha}_m = a(pt_{uni})^b, \tag{13}$$

TABLE 2 Ground motion database used in the analyses

Record	Magnitude [M_w]	Mechanism	Rjb [km]	Rrup [km]	Vs30 [m/s]	Lowest usable frequency [Hz]
1,004	6.69	Reverse	0	8.44	380.06	0.182
1,050	6.69	Reverse	4.92	7.01	2,016.13	0.16
1,052	6.69	Reverse	5.26	7.26	508.08	0.14
1,119	6.9	Strike slip	0	0.27	312	0.1625
1,120	6.9	Strike slip	1.46	1.47	256	0.125
148	5.74	Strike slip	6.75	7.42	349.85	0.1625
149	5.74	Strike slip	4.79	5.7	221.78	0.15
3,548	6.93	Reverse oblique	3.22	5.02	1070.34	0.1
4,040	6.6	Strike slip	0.05	1.7	487.4	0.0625
4,097	6	Strike slip	1.6	2.99	648.09	0.125
4,101	6	Strike slip	4.95	5.55	397.36	0.4125
4,103	6	Strike slip	3.3	4.23	410.4	0.15
4,228	6.63	Reverse	6.27	8.93	375	0.05
4,451	7.1	Reverse	0	6.98	462.23	0.25
4,458	7.1	Reverse	3.97	5.76	318.74	0.1625
4,482	6.3	Normal	0	6.55	552	0.0625
451	6.19	Strike slip	0.18	0.53	561.43	0.125
459	6.19	Strike slip	9.85	9.87	663.31	0.1625
566	5.4	Normal	4	5.6	382.21	0.1625
568	5.8	Strike slip	2.14	6.3	489.34	0.125
77	6.61	Reverse	0	1.81	2,016.13	0.0875

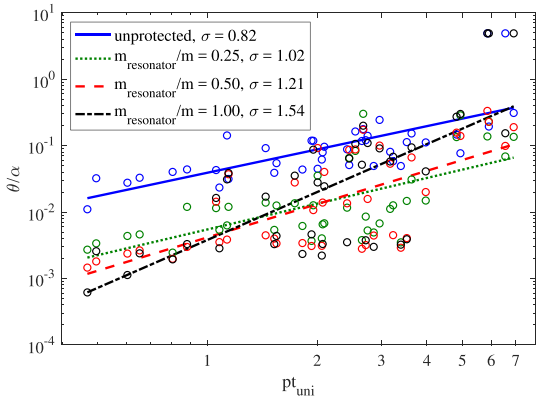

FIGURE 14 Seismic demand analysis of a rocking body ($\alpha = 18.5^o$, w = 2 m) subjected to the suite of records described in Table 2. Unprotected refers to systems without external resonators. No supplemental rotational inertia is present (i.e., $m_{inerter} = 0$). σ is the corresponding standard deviation

which becomes a linear function in the logarithmic plane

$$\ln\left(\overline{\theta/\alpha}_m\right) = \ln(a) + b\ \ln\left(pt_{uni}\right), \tag{14}$$

where a and b are the linear regression coefficients obtained by least squares procedures. Although not significant in number, overturning cases are not considered for the regression analyses. Importantly, these regression models are not offered as predictive tools but rather as a means for a qualitative comparison of potential improvements when the non-coherent components of realistic records are accounted for. In fact, the simplicity of the regression models employed is associated with noticeable levels of dispersion; however, the main trends and relative improvements are still appreciable from the corresponding figures.

Figure 14 presents the results of the cloud analyses and the corresponding seismic demand models for rocking blocks protected with external resonators of different effective masses and without supplemental inertia devices. Overall, the systems equipped with external resonators show major reductions in seismic demands for the whole range of pt_{uni} studied in comparison with unprotected structures. Reductions of around one order of magnitude are observed for low pt_{uni} values when the external resonators are employed (Figure 14). These large levels of vibration absorption are maintained over the full frequency range when resonator masses of 25% or 50% of the structural mass are employed. On the other hand, the larger resonator mass of $m_{resonator} = 1m$, although still effective in reducing peak rotations, becomes progres-

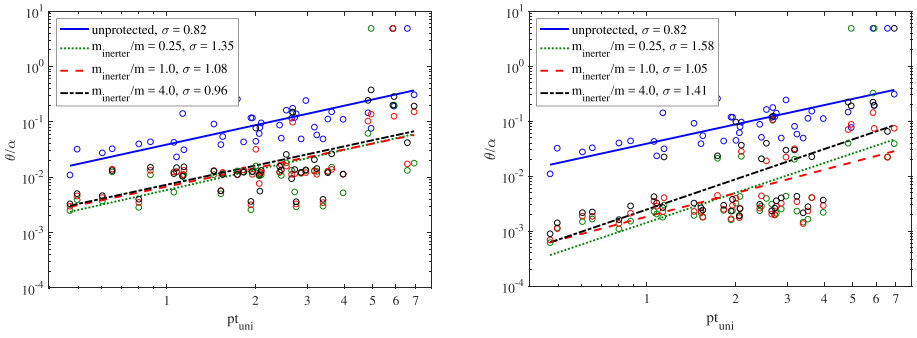

(A) $m_{resonator} = 0.25m$. **(B)** $m_{resonator} = 0.50m$.

FIGURE 15 Seismic demand analysis of a rocking body ($\alpha = 18.5^o$, w = 2 m) subjected to the suite of records described in Table 2 with different levels of supplemental rotational inertia. Unprotected refers to systems without external resonators. σ is the corresponding standard deviation

sively less effective at larger pt_{uni} values. This confirms the observation made above regarding the existence of an optimal supplemental mass quantity above which the resonators lose their vibration control efficiency. The occasions of block overturning ($\theta/\alpha > 1$), not considered in the regression analysis, are also reduced from 2 in the unprotected case to 1 in the protected structure with $m_{resonator} = 1m$ and completely avoided in the $m_{resonator} = 0.25m$ and $m_{resonator} = 0.5m$ configurations.

The case study for systems with coupled inerter-vibration absorber devices shown in Figure 15 provides further evidence for the significant improvements on the seismic response of rocking structures brought about by the external vibrating masses. The improvements are higher when an effective mass of 50% of the total structural mass is employed in the resonator (Figure 15B) in comparison with the $m_{resonator} = 0.25m$ configuration (Figure 15A). This level of supplemental mass ($m_{resonator}/m = 0.5$) can lead to 85% smaller rotations at the short pt_{uni} range. As before, the relationship between the total amount of inertial mass ($m_{resonator} + m_{inerter}$) and the rotation reduction is not linear and very large inertance values (e.g., $m_{inerter}/m = 4$ in Figure 15A,C) are found to be suboptimal. Nevertheless, in the cases studied in this section, no counter-productive effects are noticed even for the largest combination of $m_{resonator}$ and $m_{inerter}$.

6 | CONCLUSIONS

This paper has examined the feasibility of employing external resonators to mitigate the rotational demands in rocking structures. Our study builds on a previously proposed system that employs vibrating masses detached from the main structure and buried in the adjacent soil interacting with it to control the seismic motion of the superstructure. These devices can be coupled with inerters in order to keep the levels of supplemental mass low while maintaining, or improving, the motion-control capabilities of the external resonators. We have shown, by means of numerical analyses and parametric studies, that the solution proposed is able to bring about significant reductions on the rotational demands experienced by rigid rocking structures. Our analyses also revealed the existence of frequency thresholds, f_p/p_{lim}, below which the effects of the external resonator can be detrimental. Besides, the rotational demands of structures with resonators are found to be less sensitive to the pulse intensity or the block slenderness, particularly in the high-frequency spectral region.

Based on numerical results employing a series of coherent pulses, we investigated the influence of important system parameters. A nonlinear relationship between resonator mass and mitigation efficiency was found with larger masses usually extending the range of efficiency of the resonators towards proportionally lower frequencies. However, resonator masses above the $m_{resonator} = m$ level become less effective in the short frequency range for blocks of slenderness $\alpha = 1/3$ with very large resonator masses being progressively less able to control rocking. On the other hand, larger masses are required to control the response of more slender blocks (e.g., $\alpha = 1/6$ and $1/9$). Some of this mass can be delivered by supplemental rotational devices although we found evidence of the existence of an optimal value of the inerter apparent mass beyond which the potential benefits of the external resonator are offset by the large forces and interactions brought about by the inerter. By contrast, provided that a stiff enough connector—able to transfer the forces generated in the resonator, hence engaging the SSRI interaction—is provided, the dynamic response of the system appears less sensitive to the stiffness of the resonating system. Similarly, the results seem insensitive to reasonable variations in the levels of energy loss or viscous damping.

On the other hand, we found evidence that external resonators located in more flexible soils are able to control better the rocking of the protected structure over a wider range of frequencies leading to lower requirements of supplemental mass. As before, higher levels of energy dissipation in the soil can steer lower reductions in rocking motion. Moreover,

nonoptimal configurations of external devices can reduce the minimum amplitude of acceleration leading to overturning when subjected to pulse-like motion, specially for larger blocks or short period pulses. Further studies on the optimal design of external resonators aimed at broadening the frequency range over which their positive effects can be manifest are required.

Finally, we have conducted a comparative assessment of the seismic performance of rocking structures with and without external resonators under real near-field ground-motion records. The results of this case study confirmed the behavioural trends observed under coherent pulse excitations. Reductions of around one order of magnitude are observed for low pt_{uni} values when the external resonators are employed for this particular structure with all records scaled to PGA = 1.5 g ($a_g/g\alpha = 4.5$). The observation of an optimal supplemental mass quantity above which the resonators lose their vibration control efficiency was also corroborated in this case study. Although not significant in number, the occasions of block overturning are also reduced by the presence of the external resonators. Importantly, due to the complex system under analysis and the constraints of the parameter space studied, further examinations are required to generalize our observations; however, the solution explored in this paper appears attractive as it opens the possibility of controlling the dynamic response of rocking structures without invasive structural interventions.

ACKNOWLEDGEMENT

We would like to thank Prof Michalis Vassiliou for his insightful comments on the draft of this paper.

ORCID

Xiao Pan https://orcid.org/0000-0001-7845-0122
Christian Málaga-Chuquitaype https://orcid.org/0000-0002-2538-7374

REFERENCES

1. Asteris P, Chronopoulos M, Chrysostomou C, Varum H, Plevris V, Kyriakides N, Silva V. Seismic vulnerability assessment of historical masonry structural systems. *Eng Struct*. 2014;62:118–134.
2. Psycharis I, Papastamatiou D, Alexandris A. Parametric investigation of the stability of classical columns under harmonic and earthquake excitations. *Earthq Eng Struct Dyn*. 2000;29(8):1093–1109.
3. Lagomarsino S. Seismic assessment of rocking masonry structures. *Bull Earthq Eng*. 2015;13(1):97–128.
4. Konstantinidis D, Makris N. Seismic response analysis of multidrum classical columns. *Earthq Eng Struct Dyn*. 2005;34(10):1243–1270.
5. Makris N, Konstantinidis D. The rocking spectrum and the limitations of practical design methodologies. *Earthq Eng Struct Dyn*. 2003;32(2):265–289.
6. Giouvanidis A, Dimitrakopoulos E. Nonsmooth dynamic analysis of sticking impacts in rocking structures. *Bull Earthq Eng*. 2017;15(5):2273–2304.
7. R RTruniger, Vassiliou M, Stojadinovic B. An analytical model of a deformable cantilever structure rocking on a rigid surface: experimental validation. *Earthq Eng Struct Dyn*. 2015;44(15):2795–2815.
8. Housner G. The behavior of inverted pendulum structures during earthquakes. *Bull Seismol Soc Amer*. 1963;53:403–417.
9. Bachmann J, Strand M, Vassiliou M, Broccardo M, Stojadinovic B. Is rocking motion predictable? *Earthq Eng Struct Dyn*. 2018;47:535–552.
10. Zhang J, Makris N. Rocking response of free-standing blocks under cycloidal pulses. *J Eng Mech*. 2001;127(5):473–483.
11. Spanos P. D., Koh A-S. Rocking of rigid blocks due to harmonic shaking. *J Eng Mech*. 1984;110(11):1627–1642.
12. Taniguchi T. Non-linear response analyses of rectangular rigid bodies subjected to horizontal and vertical ground motion. *Earthq Eng Struct Dyn*. 2002;31(8):1481–1500.
13. Dimitrakopoulos E, DeJong M. Revisiting the rocking block: closed-form solutions and similarity laws. *Proc R Soc A: Math Phys Eng Sci*. 2012;468:2294–2318.
14. Spanos PD, Koh A-S. Analysis of block random rocking. *Soil Dyn Earthq Eng*. 1986;5(3):178–183.
15. Calio I, Marletta M. Passive control of the seismic rocking response of art objects. *Eng Struct*. 2003;25(8):1009–1018.
16. Makris N, Zhang J. Rocking response of anchored blocks under pulse-type motions. *J Eng Mech*. 2001;127:484–493.
17. deLeo A, Simoneschi G, Fabrizio C, DiEgidio A. On the use of a pendulum as mass damper to control the rocking motion of a rigid block with fixed characteristics. *Meccanica*. 2016;51(11):2727–2740.
18. Simoneschi G, de Leo AM, Di Egidio A. Effectiveness of oscillating mass damper system in the protection of rigid blocks under impulsive excitation. *Eng Struct*. 2017;137:285–295.
19. Corbi O. Laboratory investigation on sloshing water dampers coupled to rigid blocks with unilateral constraints. *Int J Mech Solids*. 2006;1(1):29–40.
20. Vassiliou M, Makris N. Analysis of the rocking response of rigid blocks standing free on a seismically isolated base. *Earthq Eng Struct Dyn*. 2012;41:177–196.

21. Thiers-Moggia R, Málaga-Chuquitaype C. Seismic protection of rocking structures with inerters. *Earthq Eng Struct Dyn*. 2019;48(5):528–547.
22. Cacciola P, Tombari A. Vibrating barrier: a novel device for the passive control of structures under ground motion. *Proc R Soc A*. 2015;471(2179):20150075.
23. Cacciola P, Tombari A, Giaralis A. A vibrating barrier with grounded inerter for non-invasive seismic protection of existing structures. In: 16th European Conference on Earthquake Engineering; 2018.
24. Makris N, Kampas G. Size versus slenderness: two competing parameters in the seismic stability of free-standing rocking columns. *Bull Seismol Soc Amer*. 2016;106(1):104–122.
25. McKenna F, Fenves GL, Scott MH, et al. *Open system for earthquake engineering simulation*. Berkeley, CA: University of California; 2000.
26. Vassiliou M, Mackie K, Stojadinović B. A finite element model for seismic response analysis of deformable rocking frames. *Earthq Eng Struct Dyn*. 2017;46(3):447–466.
27. Hilber H, Hughes T, Taylor R. Improved numerical dissipation for time integration algorithms in structural dynamics. *Earthq Eng Struct Dyn*. 1977;5(3):283–292.
28. Spieth H, Carr A, Murahidy A, Arnolds D, Davies M, Mander J. Modelling of post-tensioned precast reinforced concrete frame structures with rocking beam-column connections. In: 2004 NZSEE Conference; 2004.
29. Richart F, Whitman RV. Comparison of footing vibration tests with theory. *J Soil Mech Found Div*. 1967;93:143–168.
30. Kibriya L, Málaga-Chuquitaype C, Kashani M, Alexander N. Nonlinear dynamics of self-centring rocking steel frames using finite element models. *Soil Dyn Earthq Eng*. 2014;43(8):1129–1147.
31. Vassiliou M, Mackie K, Stojadinović B. A finite element model for seismic response analysis of deformable rocking frames. *Earthq Eng Struct Dyn*. 2017;46(3):447–466.
32. Gazetas G. Analysis of machine foundation vibrations: state of the art. *Int J Soil Dyn Earth Eng*. 1983;2(1):2–42.
33. Mulliken JS, Karabalis D. Discrete model for dynamic through-the-soil coupling of 3-D foundations and structures. *Earthq Eng Struct Dyn*. 1998;27(7):687–710.
34. Aldaikh H, Alexander N, Ibraim E, Oddbjornsson O. Two dimensional numerical and experimental models for the study of structure–soil–structure interaction involving three buildings. *Comput Struct*. 2015;150:79–91.
35. Alexander N, Ibraim E, Aldaikh H. A simple discrete model for interaction of adjacent buildings during earthquakes. *Comput Struct*. 2013;124:1–10.
36. Gazetas G. Analysis of machine foundation vibrations: state of the art. *Int J Soil Dyn Earthq Eng*. 1983;2(1):2–42.
37. Arakaki T, Kuroda H, Arima F, Inoue Y, Baba K. Development of seismic devices applied to ball screw. Part 1: basic performance of test RD-series. *AIJ JTechnol Des*. 1999;8:239–244.
38. Smith M. Synthesis of mechanical networks: the inerter. *IEEE T Automat Contr*. 2002;47(10):1648–1662.
39. Papageorgiou C, Smith MC. Laboratory experimental testing of inerters. In: Proceedings of the 44th IEEE Conference on Decision and Control IEEE; 2005:3351–3356.
40. Takewaki I, Murakami S, Yoshitomi S, Tsuji M. Fundamental mechanism of earthquake response reduction in building structures with inertial dampers. *Struct Control Health Monit*. 2012;19(6):590–608.
41. Málaga-Chuquitaype C, Menendez-Vicente C, Thiers-Moggia R. Experimental and numerical assessment of the seismic response of steel structures with clutched inerters. *Soil Dyn Earthq Eng*. 2019;121:200–211.
42. Mavroeidis GP, Papageorgiou AS. A mathematical representation of near-fault ground motions. *Bull Seismol Soc Amer*. 2003;93(3):1099–131.
43. Málaga-Chuquitaype C, Psaltakis M, Kampas G, Wu J. Dimensionless fragility analysis of seismic acceleration demands through low-order building models. *Bull Earthq Eng*. 2019;17(7):3815–3845.
44. Dimitrakopoulos E, Fung EDW. Closed-form rocking overturning conditions for a family of pulse ground motions. *Proc R Soc A Math Phys Eng Sci*. 2016;472(2196):20160662.
45. Vaschy A. Sur les lois de similitude en physique. *Annales Telegraphiques*. 1892;19:25–28.
46. Buckingham E. Model experiments and the forms of empirical equations. *Trans Amer Soc Mech Eng*. 1915;37:263–296.
47. Lagomarsino S, Abbas N, Calderini C, et al. Classification of cultural heritage assets and seismic damage variables for the identification. *WIT Trans Built Env*. 2011;118:697–708.
48. Kržan M, Gostič S, Cattari S, Bosiljkov V. Acquiring reference parameters of masonry for the structural performance analysis of historical buildings. *Bull Earthq Eng*. 2015;13(1):203–236.
49. Ikago K, Saito K, Inoue N. Seismic control of single-degree-of-freedom structure using tuned viscous damper. *Earthq Eng Struct Dyn*. 2012;41(3):436–474.
50. Dimitrakopoulos E, Giouvanidis A. Rocking amplification and strong-motion duration. *Earthq Eng Struct Dyn*. 2018;47(10):1–22.

How to cite this article: Pan X, Málaga-Chuquitaype C. Seismic control of rocking structures via external resonators. *Earthquake Engng Struct Dyn*. 2020;49:1180-1196. https://doi.org/10.1002/eqe.3284